Title
Search for muon neutrinos from Gamma-Ray Bursts with the IceCube neutrino telescope

Permalink
https://escholarship.org/uc/item/3dd7q99s

Author
Abbasi, R.

Publication Date
2010

Search for muon neutrinos from Gamma-Ray Bursts with the IceCube neutrino telescope

R. Abbasi, etal

[1]Dept. of Physics, University of Wisconsin, Madison, WI 53706, USA
[2]Dept. of Subatomic and Radiation Physics, University of Gent, B-9000 Gent, Belgium
[3]Dept. of Physics, University of Wisconsin, River Falls, WI 54022, USA
[4]Dept. of Physics and Astronomy, University of Canterbury, Private Bag 4800, Christchurch, New Zealand
[5]Dept. of Physics, University of Oxford, 1 Keble Road, Oxford OX1 3NP, UK
[6]Dept. of Physics, University of Wuppertal, D-42119 Wuppertal, Germany
[7]Bartol Research Institute and Department of Physics and Astronomy, University of Delaware, Newark, DE 19716, USA
[8]Dept. of Physics and Astronomy, University of California, Irvine, CA 92697, USA
[9]Dept. of Physics, University of California, Berkeley, CA 94720, USA
[10]DESY, D-15735 Zeuthen, Germany
[11]Lawrence Berkeley National Laboratory, Berkeley, CA 94720, USA
[12]Dept. of Physics and Center for Cosmology and Astro-Particle Physics, Ohio State University, Columbus, OH 43210, USA
[13]Dept. of Astronomy, Ohio State University, Columbus, OH 43210, USA
[14]Universit´e Libre de Bruxelles, Science Faculty CP230, B-1050 Brussels, Belgium
[15]Dept. of Physics, TU Dortmund University, D-44221 Dortmund, Germany
[16]Dept. of Physics, University of Maryland, College Park, MD 20742, USA
[17]Dept. of Physics and Astronomy, University of Kansas, Lawrence, KS 66045, USA
[18]III Physikalisches Institut, RWTH Aachen University, D-52056 Aachen, Germany
[19]Oskar Klein Centre and Dept. of Physics, Stockholm University, SE-10691 Stockholm, Sweden
[20]Dept. of Physics and Astronomy, Uppsala University, Box 516, S-75120 Uppsala, Sweden
[21]Dept. of Physics, Pennsylvania State University, University Park, PA 16802, USA
[22]University of Mons-Hainaut, 7000 Mons, Belgium
[23]Laboratory for High Energy Physics, ´Ecole Polytechnique F´ed´erale, CH-1015 Lausanne, Switzerland
[24]Dept. of Astronomy and Astrophysics, Pennsylvania State University, University Park, PA 16802, USA
[25]Vrije Universiteit Brussel, Dienst ELEM, B-1050 Brussels, Belgium
[26]Dept. of Physics and Astronomy, Utrecht University/SRON, NL-3584 CC Utrecht, The Netherlands
[27]CTSPS, Clark-Atlanta University, Atlanta, GA 30314, USA
[28]Dept. of Physics, Southern University, Baton Rouge, LA 70813, USA
[29]Institut f¨ur Physik, Humboldt-Universit¨at zu Berlin, D-12489 Berlin, Germany
[30]Dept. of Astronomy, University of Wisconsin, Madison, WI 53706, USA
[31]Institute of Physics, University of Mainz, Staudinger Weg 7, D-55099 Mainz, Germany
[32]Max-Planck-Institut f¨ur Kernphysik, D-69177 Heidelberg, Germany

19 Jan 2010

DISCLAIMER

Search for muon neutrinos from Gamma-Ray Bursts with the IceCube neutrino telescope

IceCube Collaboration: R. Abbasi[1], Y. Abdou[2], T. Abu-Zayyad[3], J. Adams[4], J. A. Aguilar[1], M. Ahlers[5], K. Andeen[1], J. Auffenberg[6], X. Bai[7], M. Baker[1], S. W. Barwick[8], R. Bay[9], J. L. Bazo Alba[10], K. Beattie[11], J. J. Beatty[12,13], S. Bechet[14], J. K. Becker[15], K.-H. Becker[6], M. L. Benabderrahmane[10], J. Berdermann[10], P. Berghaus[1], D. Berley[16], E. Bernardini[10], D. Bertrand[14], D. Z. Besson[17], M. Bissok[18], E. Blaufuss[16], D. J. Boersma[1], C. Bohm[19], J. Bolmont[10], O. Botner[20], L. Bradley[21], J. Braun[1], D. Breder[6], T. Castermans[22], D. Chirkin[1], B. Christy[16], J. Clem[7], S. Cohen[23], D. F. Cowen[21,24], M. V. D'Agostino[9], M. Danninger[19], C. T. Day[11], C. De Clercq[25], L. Demirörs[23], O. Depaepe[25], F. Descamps[2], P. Desiati[1], G. de Vries-Uiterweerd[2], T. DeYoung[21], J. C. Diaz-Velez[1], J. Dreyer[15], J. P. Dumm[1], M. R. Duvoort[26], W. R. Edwards[11], R. Ehrlich[16], J. Eisch[1], R. W. Ellsworth[16], O. Engdegård[20], S. Euler[18], P. A. Evenson[7], O. Fadiran[27], A. R. Fazely[28], T. Feusels[2], K. Filimonov[9], C. Finley[1], M. M. Foerster[21], B. D. Fox[21], A. Franckowiak[29], R. Franke[10], T. K. Gaisser[7], J. Gallagher[30], R. Ganugapati[1], L. Gerhardt[11,9], L. Gladstone[1], A. Goldschmidt[11], J. A. Goodman[16], R. Gozzini[31], D. Grant[21], T. Griesel[31], A. Groß[4,32], S. Grullon[1], R. M. Gunasingha[28], M. Gurtner[6], C. Ha[21], A. Hallgren[20], F. Halzen[1], K. Han[4], K. Hanson[1], Y. Hasegawa[33], J. Heise[26], K. Helbing[6], P. Herquet[22], S. Hickford[4], G. C. Hill[1], K. D. Hoffman[16], K. Hoshina[1], D. Hubert[25], W. Huelsnitz[16], J.-P. Hülß[18], P. O. Hulth[19], K. Hultqvist[19], S. Hussain[7], R. L. Imlay[28], M. Inaba[33], A. Ishihara[33], J. Jacobsen[1], G. S. Japaridze[27], H. Johansson[19], J. M. Joseph[11], K.-H. Kampert[6], A. Kappes[1,34], T. Karg[6], A. Karle[1], J. L. Kelley[1], P. Kenny[17], J. Kiryluk[11,9], F. Kislat[10], S. R. Klein[11,9], S. Knops[18], G. Kohnen[22], H. Kolanoski[29], L. Köpke[31], M. Kowalski[29], T. Kowarik[31], M. Krasberg[1], K. Kuehn[12], T. Kuwabara[7], M. Labare[14], S. Lafebre[21], K. Laihem[18], H. Landsman[1], R. Lauer[10], D. Lennarz[18], A. Lucke[29], J. Lundberg[20], J. Lünemann[31], J. Madsen[3], P. Majumdar[10], R. Maruyama[1], K. Mase[33], H. S. Matis[11], C. P. McParland[11], K. Meagher[16], M. Merck[1], P. Mészáros[24,21], E. Middell[10], N. Milke[15], H. Miyamoto[33], A. Mohr[29], T. Montaruli[1,35], R. Morse[1], S. M. Movit[24], R. Nahnhauer[10], J. W. Nam[8], P. Nießen[7], D. R. Nygren[11,19], S. Odrowski[32], A. Olivas[16], M. Olivo[20], M. Ono[33], S. Panknin[29], S. Patton[11], C. Pérez de los Heros[20], J. Petrovic[14], A. Piegsa[31], D. Pieloth[15], A. C. Pohl[20,36], R. Porrata[9], N. Potthoff[6], P. B. Price[9], M. Prikockis[21], G. T. Przybylski[11], K. Rawlins[37], P. Redl[16], E. Resconi[32], W. Rhode[15], M. Ribordy[23], A. Rizzo[25], J. P. Rodrigues[1], P. Roth[16], F. Rothmaier[31], C. Rott[12], C. Roucelle[32], D. Rutledge[21], D. Ryckbosch[2], H.-G. Sander[31], S. Sarkar[5], S. Schlenstedt[10], T. Schmidt[16], D. Schneider[1], A. Schukraft[18], O. Schulz[32], M. Schunck[18], D. Seckel[7], B. Semburg[6], S. H. Seo[19], Y. Sestayo[32], S. Seunarine[4], A. Silvestri[8], A. Slipak[21], G. M. Spiczak[3], C. Spiering[10], M. Stamatikos[12], T. Stanev[7], G. Stephens[21], T. Stezelberger[11], R. G. Stokstad[11], M. C. Stoufer[11], S. Stoyanov[7], E. A. Strahler[1], T. Straszheim[16], K.-H. Sulanke[10], G. W. Sullivan[16], Q. Swillens[14], I. Taboada[38], A. Tamburro[3], O. Tarasova[10], A. Tepe[6], S. Ter-Antonyan[28], C. Terranova[23], S. Tilav[7], P. A. Toale[21], J. Tooker[38], D. Tosi[10], D. Turčan[16], N. van Eijndhoven[26], J. Vandenbroucke[9], A. Van Overloop[2], B. Voigt[10], C. Walck[19], T. Waldenmaier[29], M. Walter[10], C. Wendt[1], S. Westerhoff[1], N. Whitehorn[1],

C. H. Wiebusch[18], A. Wiedemann[15], G. Wikström[19], D. R. Williams[39], R. Wischnewski[10], H. Wissing[18,16], K. Woschnagg[9], X. W. Xu[28], G. Yodh[8], and S. Yoshida[33]

– 3 –

[1]Dept. of Physics, University of Wisconsin, Madison, WI 53706, USA

[2]Dept. of Subatomic and Radiation Physics, University of Gent, B-9000 Gent, Belgium

[3]Dept. of Physics, University of Wisconsin, River Falls, WI 54022, USA

[4]Dept. of Physics and Astronomy, University of Canterbury, Private Bag 4800, Christchurch, New Zealand

[5]Dept. of Physics, University of Oxford, 1 Keble Road, Oxford OX1 3NP, UK

[6]Dept. of Physics, University of Wuppertal, D-42119 Wuppertal, Germany

[7]Bartol Research Institute and Department of Physics and Astronomy, University of Delaware, Newark, DE 19716, USA

[8]Dept. of Physics and Astronomy, University of California, Irvine, CA 92697, USA

[9]Dept. of Physics, University of California, Berkeley, CA 94720, USA

[10]DESY, D-15735 Zeuthen, Germany

[11]Lawrence Berkeley National Laboratory, Berkeley, CA 94720, USA

[12]Dept. of Physics and Center for Cosmology and Astro-Particle Physics, Ohio State University, Columbus, OH 43210, USA

[13]Dept. of Astronomy, Ohio State University, Columbus, OH 43210, USA

[14]Université Libre de Bruxelles, Science Faculty CP230, B-1050 Brussels, Belgium

[15]Dept. of Physics, TU Dortmund University, D-44221 Dortmund, Germany

[16]Dept. of Physics, University of Maryland, College Park, MD 20742, USA

[17]Dept. of Physics and Astronomy, University of Kansas, Lawrence, KS 66045, USA

[18]III Physikalisches Institut, RWTH Aachen University, D-52056 Aachen, Germany

[19]Oskar Klein Centre and Dept. of Physics, Stockholm University, SE-10691 Stockholm, Sweden

[20]Dept. of Physics and Astronomy, Uppsala University, Box 516, S-75120 Uppsala, Sweden

[21]Dept. of Physics, Pennsylvania State University, University Park, PA 16802, USA

[22]University of Mons-Hainaut, 7000 Mons, Belgium

[23]Laboratory for High Energy Physics, École Polytechnique Fédérale, CH-1015 Lausanne, Switzerland

[24]Dept. of Astronomy and Astrophysics, Pennsylvania State University, University Park, PA 16802, USA

[25]Vrije Universiteit Brussel, Dienst ELEM, B-1050 Brussels, Belgium

[26]Dept. of Physics and Astronomy, Utrecht University/SRON, NL-3584 CC Utrecht, The Netherlands

[27]CTSPS, Clark-Atlanta University, Atlanta, GA 30314, USA

[28]Dept. of Physics, Southern University, Baton Rouge, LA 70813, USA

[29]Institut für Physik, Humboldt-Universität zu Berlin, D-12489 Berlin, Germany

[30]Dept. of Astronomy, University of Wisconsin, Madison, WI 53706, USA

[31]Institute of Physics, University of Mainz, Staudinger Weg 7, D-55099 Mainz, Germany

[32]Max-Planck-Institut für Kernphysik, D-69177 Heidelberg, Germany

ABSTRACT

We present the results of searches for high-energy muon neutrinos from 41 gamma-ray bursts (GRBs) in the northern sky with the IceCube detector in its 22-string configuration active in 2007/2008. The searches cover both the prompt and a possible precursor emission as well as a model-independent, wide time window of $-1\,\mathrm{h}$ to $+3\,\mathrm{h}$ around each GRB. In contrast to previous searches with a large GRB population, we do not utilize a standard Waxman–Bahcall GRB flux for the prompt emission but calculate individual neutrino spectra for all 41 GRBs from the burst parameters measured by satellites. For all three time windows the best estimate for the number of signal events is zero. Therefore, we place 90% CL upper limits on the fluence from the prompt phase of $3.7 \times 10^{-3}\,\mathrm{erg\,cm^{-2}}$ ($72\,\mathrm{TeV}$ – $6.5\,\mathrm{PeV}$) and on the fluence from the precursor phase of $2.3 \times 10^{-3}\,\mathrm{erg\,cm^{-2}}$ ($2.2\,\mathrm{TeV}$ – $55\,\mathrm{TeV}$), where the quoted energy ranges contain 90% of the expected signal events in the detector. The 90% CL upper limit for the wide time window is $2.7 \times 10^{-3}\,\mathrm{erg\,cm^{-2}}$ ($3\,\mathrm{TeV}$ – $2.8\,\mathrm{PeV}$) assuming an E^{-2} flux.

Subject headings: gamma-ray bursts: general – methods: data analysis – neutrinos – telescopes

1. Introduction

Gamma-ray bursts (GRBs) are among the most violent events in the universe and among the few plausible candidates for sources of the ultra-high energy cosmic rays. So-called long-duration GRBs ($\gtrsim 2\,\mathrm{s}$) are thought to originate from the collapse of a massive star into a black hole (Woosley 1993), whereas short-duration GRBs ($\lesssim 2\,\mathrm{s}$) are believed to be the result of the merger of two compact objects (e.g., neutron stars) into a black hole (Eichler et al. 1989). Though quite different in nature both scenarios are consistent with the currently leading model for GRBs, the fireball model (Meszaros & Rees 1993), with the energy source (central engine) being the rapid

[33] Dept. of Physics, Chiba University, Chiba 263-8522, Japan

[34] affiliated with Universität Erlangen-Nürnberg, Physikalisches Institut, D-91058, Erlangen, Germany

[35] on leave of absence from Università di Bari and Sezione INFN, Dipartimento di Fisica, I-70126, Bari, Italy

[36] affiliated with School of Pure and Applied Natural Sciences, Kalmar University, S-39182 Kalmar, Sweden

[37] Dept. of Physics and Astronomy, University of Alaska Anchorage, 3211 Providence Dr., Anchorage, AK 99508, USA

[38] School of Physics and Center for Relativistic Astrophysics, Georgia Institute of Technology, Atlanta, GA 30332. USA

[39] Dept. of Physics and Astronomy, University of Alabama, Tuscaloosa, AL 35487, USA

accretion of a large mass onto the newly formed black hole. In this model, a highly relativistic outflow (fireball) dissipates its energy via synchrotron or inverse Compton radiation of electrons accelerated in internal shock fronts (Narayan et al. 1992; Rees & Meszaros 1994; Sari & Piran 1997). This radiation in the keV–MeV range is observed as the γ-ray signal. In case of long GRBs the energy in gamma rays is typically of $\mathcal{O}(10^{51}$–$10^{54}\,\mathrm{erg} \times \Omega/4\pi)$ where Ω is the opening angle for the γ-ray emission. Short GRBs are observed to release about a factor 100 less energy.

In addition to electrons, protons are thought to be accelerated via the Fermi mechanism, resulting in an E^{-2} power law spectrum with energies up to $10^{20}\,\mathrm{eV}$ (Waxman 1995; Vietri 1995). The normalization of the proton spectrum is usually given in relation to the energy in electrons. The latter is linked to the energy in γ-ray photons through the synchrotron and inverse Compton energy-loss mechanisms. Protons of $\mathcal{O}(10^{15}\,\mathrm{eV})$ interact with the keV–MeV photons forming a Δ^+ resonance which decays into pions (Waxman & Bahcall 1997). In the decay of the charged pions, neutrinos of energy $\mathcal{O}(10^{14}\,\mathrm{eV})$ are produced with the approximate ratios $(\nu_e{:}\nu_\mu{:}\nu_\tau) = (1{:}2{:}0)$ [1], changing to about (1:1:1) at Earth due to oscillations (Learned & Pakvasa 1995; Athar et al. 2006). First calculations of this prompt neutrino flux (Waxman & Bahcall 1997; Alvarez-Muniz & Halzen 1999) used average GRB parameters and the GRB rate measured by BATSE to determine an all-sky neutrino flux from the GRB population. The AMANDA-II neutrino telescope (Achterberg et al. 2007, 2008) performed searches for this so-called Waxman–Bahcall GRB flux or similar GRB fluxes (Achterberg et al. 2007, 2008) with negative results.

In a similar way, so-called precursor neutrinos can be generated when the expanding fireball is still inside the progenitor star (Razzaque et al. 2003). In this case, the accelerated protons interact with matter of the progenitor star or synchrotron photons. However, due to the large optical depth the synchrotron photons cannot escape the fireball and, hence, no γ-ray signal is observed. The time delay between the start of this neutrino emission and the prompt γ-ray signal is expected to be about $100\,\mathrm{s}$.

Observations of the early and late afterglow phases reveal that a large fraction of GRBs show X-ray flares superposed on the decaying light curve. Sometimes these flares are interpreted as a restart of the central engine that already generated the prompt emission (Burrows et al. 2007). If this is true, neutrino production with a similar spectrum as the prompt emission can be expected in the afterglow phase up to $10^4\,\mathrm{s}$ after the γ-ray signal (Murase & Nagataki 2006). Furthermore, production of neutrinos with energies around $10^{18}\,\mathrm{GeV}$ is expected when the shock fronts collide with the interstellar medium or the progenitor wind (Waxman & Bahcall 2000).

In our analysis we search for muon neutrinos from GRBs recorded by satellites between 2007 June 1 and 2008 April 4 in all three phases. For the prompt phase we utilize both an unbinned likelihood and a binned method. We find that the unbinned likelihood method has a significantly better discovery potential and is therefore used to obtain the limits presented in this paper. For

---

[1]Here and throughout the rest of the paper ν denotes both neutrinos and antineutrinos.

searches in other emission phases we perform only an unbinned search. The paper is structured as follows: In Section 2 we define the neutrino spectra used for the different phases, followed by a description of the IceCube detector in Section 3. Afterwards, in Sections 4 and 5 the data sets and simulations are discussed, respectively. In Section 6 the unbinned likelihood and binned methods are described and their performance is compared. Section 7 then presents the results followed by a discussion of systematic uncertainties. Finally, Section 8 sets the results into context with other observations.

2. GRB neutrino-spectra and time windows

The searches in this paper rely on the directional, temporal and spectral information obtained from satellite-based γ-ray observations which are distributed via the Gamma-ray burst Coordinate Network (GCN, NASA (2009)). Primarily, this information comes from *Swift* (Burrows et al. 2005) (also X-ray and UV observations), but also from Konus-Wind (NASA 1994), SuperAGILE (Tavani et al. 2008), Integral (Mereghetti 2004), and other satellites of the Third Interplanetary Network (IPN 1990). In our analyses we only consider bursts which occurred at a declination above $-5°$. The southern sky is dominated by downgoing muons created by cosmic ray interactions with the atmosphere. By restricting our searches to the northern sky, the background from downward going muons is drastically reduced. The resolution of the GRB position from the satellites is better than $0.1°$, well below the resolution of the IceCube detector. It is therefore neglected in these analyses.

2.1. Prompt emission

We calculate the expected prompt neutrino spectrum in the internal shock scenario of the fireball model following Guetta et al. (2004) which is based on Waxman & Bahcall (1997). For reference we list all formulae used in our calculations in Appendix A together with a definition of the various parameters. Prompt neutrino emission from GRBs is the result of meson production in collisions of accelerated protons and the observed γ-rays in the keV–MeV range. It is therefore expected to occur during the same time frame as the γ-ray emission and to track the photon energy spectrum. This is reflected in the similar functional form of F_γ (Equation (A1)) and F_ν (Equation (A3)). Due to the Δ^+ resonance condition, the neutrino energy is predicted to be inversely proportional to the photon energy, which is illustrated in the definition of α_ν and β_ν in Equation (A6). The further break in the neutrino spectrum above an energy ϵ_2 is due to synchrotron cooling of high energy pions and muons before producing neutrinos. The expected energy fluence in neutrinos is directly proportional to the measured energy fluence in photons (Equation (A8)). Here, some of the measured photon indices lead to diverging γ-ray spectral integrals if integrated from zero to infinity in energy. As the photon spectrum will not follow a broken power law spectrum to arbitrarily high or low energies, we limit the integration range for all GRBs from $1\,\mathrm{keV}$ to $10\,\mathrm{MeV}$ for which broken power law spectra have been observed by γ-ray satellites.

Table 1.   Burst Parameters, γ-Ray and Neutrino Spectra of All 41 GRBs (for Definitions of Parameters See Appendix A)

	General Burst Parameters						γ-Ray Spectrum				ν Spectrum					
	T_0	R.A.	Decl.	T_1-T_0	T_2-T_0	z	f_γ	ϵ_γ	α_γ	β_γ	f_ν	$\epsilon_{\nu,1}$	$\epsilon_{\nu,2}$	α_ν	β_ν	γ_ν
GRB 070610	20:52:26	298.8	26.2	-0.8	$+4.4$	2.00^*	2.3e+00	0.20^*	1.76	2.76^*	2.2e$-$17	0.35	8.54	0.24	1.24	3.24
GRB 070612A	02:38:45	121.4	37.3	-4.7	$+418.0$	2.00^*	1.1e+02	0.20^*	1.69	2.69^*	1.2e$-$15	0.35	8.54	0.31	1.31	3.31
GRB 070616	16:29:33	32.2	56.9	-2.6	$+602.2$	2.00^*	2.2e+02	0.20^*	1.61	2.61^*	2.8e$-$15	0.35	8.54	0.39	1.39	3.39
GRB 070704	20:05:57	354.7	66.3	-57.3	$+400.8$	2.00^*	5.4e+01	0.20^*	1.79	2.79^*	4.9e$-$16	0.35	8.54	0.21	1.21	3.21
GRB 070714B	04:59:29	57.8	28.3	-0.8	$+65.6$	0.92	1.1e+01	0.20^*	1.36	2.36^*	5.1e$-$17	0.85	13.34	0.64	1.64	3.64
GRB 070724B	23:25:09	17.6	57.7	-2.0	$+120.0$	2.00^*	1.1e+03	0.08	1.15	3.15	1.8e$-$15	0.85	8.54	-0.15	1.85	3.85
GRB 070808	18:28:00	6.8	1.2	-0.7	$+41.4$	2.00^*	1.6e+01	0.20^*	1.47	2.47^*	2.8e$-$16	0.35	8.54	0.53	1.53	3.53
GRB 070810B	15:19:17	9.0	8.8	$+0.0$	$+0.1$	2.00^*	1.4e$-$01	0.20^*	1.44	2.44^*	2.6e$-$18	0.35	8.54	0.56	1.56	3.56
GRB 070917	07:33:57	293.9	2.4	-0.1	$+11.4$	2.00^*	3.7e+01	0.21	1.36	3.36	6.0e$-$16	0.33	8.54	-0.36	1.64	3.64
GRB 070920A	04:00:13	101.0	72.3	$+15.1$	$+75.0$	2.00^*	5.3e+00	0.20^*	1.69	2.69^*	5.7e$-$17	0.35	8.54	0.31	1.31	3.31
GRB 071003	07:40:55	301.9	10.9	-7.6	$+167.4$	2.00^*	3.0e+01	0.80	0.97	2.97	3.8e$-$14	0.09	8.54	0.03	2.03	4.03
GRB 071008	21:55:56	151.6	44.3	-11.0	$+14.0$	2.00^*	1.2e+00	0.20^*	2.23	3.23^*	6.4e$-$18	0.35	8.54	-0.23	0.77	2.77
GRB 071010B	20:45:47	150.5	45.7	-35.7	$+24.1$	0.95	2.1e+03	0.03	1.25	2.65	5.0e$-$17	5.71	13.16	0.35	1.75	3.75
GRB 071010C	22:20:22	338.1	66.2	-2.0	$+20.0$	2.00^*	$3.2e+01^*$	0.20^*	1.00^*	2.00^*	1.8e$-$15	0.35	8.54	1.00	2.00	4.00
GRB 071011	12:40:13	8.4	61.1	-9.5	$+63.8$	2.00^*	3.2e+01	0.20^*	1.41	2.41^*	6.3e$-$16	0.35	8.54	0.59	1.59	3.59
GRB 071013	12:09:19	279.5	33.9	-5.9	$+23.4$	2.00^*	3.7e+00	0.20^*	1.60	2.60^*	4.8e$-$17	0.35	8.54	0.40	1.40	3.40
GRB 071018	08:37:41	164.7	53.8	-50.0	$+417.7$	2.00^*	1.1e+01	0.20^*	1.63	2.63^*	1.4e$-$16	0.35	8.54	0.37	1.37	3.37
GRB 071020	07:02:27	119.7	32.9	-3.0	$+7.4$	2.15	2.6e+01	0.32	0.65	2.65	5.3e$-$15	0.20	8.13	0.35	2.35	4.35
GRB 071021	09:41:33	340.6	23.7	-31.4	$+252.2$	2.00^*	1.3e+01	0.20^*	1.70	2.70^*	1.4e$-$16	0.35	8.54	0.30	1.30	3.30
GRB 071025	04:08:54	355.1	31.8	$+38.5$	$+193.8$	2.00^*	5.9e+01	0.20^*	1.79	2.79^*	5.4e$-$16	0.35	8.54	0.21	1.21	3.21
GRB 071028A	17:41:01	119.8	21.5	$+0.0$	$+48.9$	2.00^*	2.4e+00	0.20^*	1.87	2.87^*	2.0e$-$17	0.35	8.54	0.13	1.13	3.13
GRB 071101	17:53:46	48.2	62.5	-1.9	$+10.0$	2.00^*	3.7e$-$01	0.20^*	2.25	3.25^*	2.1e$-$18	0.35	8.54	-0.25	0.75	2.75
GRB 071104	11:41:23	295.6	14.6	-5.0	$+17.0$	2.00^*	$3.2e+01^*$	0.20^*	1.00^*	2.00^*	1.8e$-$15	0.35	8.54	1.00	2.00	4.00
GRB 071109	20:36:05	289.9	2.0	-5.0	$+35.0$	2.00^*	$3.2e+01^*$	0.20^*	1.00^*	2.00^*	1.8e$-$15	0.35	8.54	1.00	2.00	4.00
GRB 071112C	18:32:57	39.2	28.4	-5.0	$+30.0$	0.82	6.3e+01	0.20^*	1.09	2.09^*	4.3e$-$16	0.95	14.07	0.91	1.91	3.91
GRB 071118	08:57:17	299.7	70.1	-25.0	$+110.0$	2.00^*	5.6e+00	0.20^*	1.63	2.63^*	6.8e$-$17	0.35	8.54	0.37	1.37	3.37
GRB 071122	01:23:25	276.6	47.1	-29.4	$+47.3$	1.14	5.4e+00	0.20^*	1.77	2.77^*	1.7e$-$17	0.69	11.97	0.23	1.23	3.23
GRB 071125	13:56:42	251.2	4.5	-0.5	$+8.5$	2.00^*	3.4e+02	0.30	0.62	3.10	3.8e$-$14	0.24	8.54	-0.10	2.38	4.38
GRB 080121	21:29:55	137.2	41.8	-0.4	$+0.4$	2.00^*	7.9e$-$02	0.20^*	2.60	3.60^*	3.6e$-$19	0.35	8.54	-0.60	0.40	2.40
GRB 080205	07:55:51	98.3	62.8	-10.1	$+105.3$	2.00^*	1.3e+01	0.20^*	2.08	3.08^*	8.0e$-$17	0.35	8.54	-0.08	0.92	2.92
GRB 080211	07:23:39	44.0	60.0	-10.0	$+50.0$	2.00^*	1.3e+02	0.35	0.61	2.62	3.1e$-$14	0.20	8.54	0.38	2.39	4.39
GRB 080218A	20:08:43	355.9	12.2	-12.8	$+18.6$	2.00^*	2.6e+00	0.20^*	2.34	3.34^*	1.3e$-$17	0.35	8.54	-0.34	0.66	2.66
GRB 080307	11:23:30	136.6	35.1	$+1.7$	$+146.1$	2.00^*	8.0e+00	0.20^*	1.78	2.78^*	7.4e$-$17	0.35	8.54	0.22	1.22	3.22
GRB 080310	08:37:58	220.1	-0.2	-71.8	$+318.0$	2.43	9.6e+00	0.20^*	2.32	3.32^*	7.2e$-$17	0.27	7.47	0.68	2.68	2.68
GRB 080315	02:25:01	155.1	41.7	-5.0	$+65.0$	2.00^*	4.3e$-$01	0.20^*	2.51	3.51^*	2.0e$-$18	0.35	8.54	-0.51	0.49	2.49
GRB 080319C	12:25:56	259.0	55.4	-0.3	$+51.2$	1.95	1.5e+02	0.11	1.01	1.87	1.8e$-$15	0.68	8.68	1.13	1.99	3.99
GRB 080319D	17:05:09	99.5	23.9	$+0.0$	$+50.0$	2.00^*	2.4e+00	0.20^*	1.92	2.92^*	1.8e$-$17	0.35	8.54	0.08	1.08	3.08
GRB 080320	04:37:38	177.7	57.2	-60.0	$+40.0$	2.00^*	2.8e+00	0.20^*	1.70	2.70^*	2.9e$-$17	0.35	8.54	0.30	1.30	3.30
GRB 080325	04:09:17	277.9	36.5	-29.3	$+170.5$	2.00^*	5.2e+01	0.20^*	1.68	2.68^*	5.7e$-$16	0.35	8.54	0.32	1.32	3.32
GRB 080328	08:03:04	80.5	47.5	-2.2	$+117.5$	2.00^*	1.0e+02	0.28	1.13	3.13	5.4e$-$15	0.25	8.54	-0.13	1.87	3.87
GRB 080330	03:41:16	169.3	30.6	-0.5	$+71.9$	1.51	1.0e+00	0.20^*	2.53	3.53^*	3.1e$-$18	0.50	10.20	-0.53	0.47	2.47

Note. — Columns: T_0 – trigger time of satellite [UT], RA – right ascension of GRB [$^\circ$], Dec – declination of GRB [$^\circ$], $T_1 - T_0$ – start of prompt window [s], $T_2 - T_0$ – end of prompt window [s], f_γ [MeV^{-1} cm^{-2}], ϵ_γ [MeV], f_ν [GeV^{-1} cm^{-2}], $\epsilon_{\nu,1}$ [PeV], $\epsilon_{\nu,2}$ [PeV]. The parameters f_γ and f_ν are the fluxes at ϵ_γ and $\epsilon_{\nu,1}$ of the gamma-ray and neutrino spectrum, respectively (see also Appendix A).

*Parameter has not been measured. Instead, an average value is used (see Table 2).

Table 2.   Average Values of GRB Parameters Taken from Becker (2008)

Parameter	Average Value
f_γ	$1.3\,\mathrm{MeV}^{-1}\,\mathrm{cm}^{-2}$ [a]
z	2
ϵ_γ	$0.2\,\mathrm{MeV}$
α_γ	1
β_γ	$\alpha_\gamma + 1$
$L_\gamma^{\mathrm{iso}*}$	$10^{51}\,\mathrm{erg}\,\mathrm{cm}^{-2}$
$\Gamma_{\mathrm{jet}}{}^*$	300
$t_{\mathrm{var}}{}^*$	$0.01\,\mathrm{s}$
$\epsilon_e{}^*$	0.1
$\epsilon_B{}^*$	0.1
$f_e{}^*$	0.1

Note. — For parameter definitions see Appendix.

[a]Corresponds to $\mathcal{F}_\gamma = 10^{-5}\,\mathrm{erg}\,\mathrm{cm}^{-2}$ between $10\,\mathrm{keV}$ and $10\,\mathrm{MeV}$.

*Not measured for any GRB.
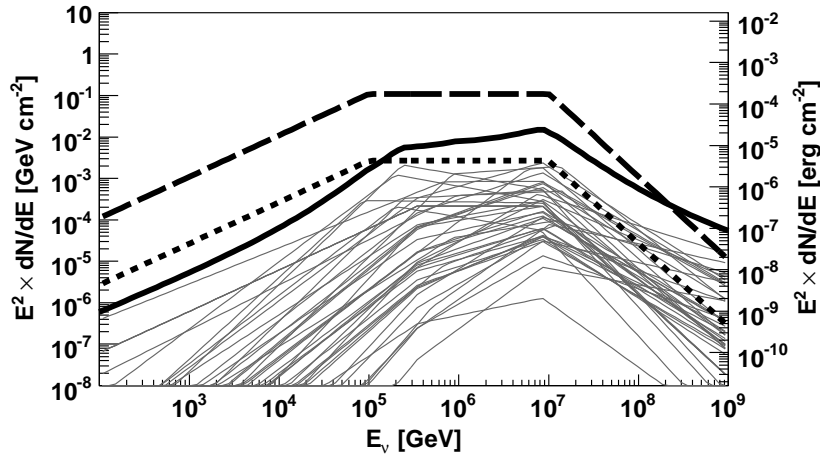
Fig. 1.— Calculated neutrino spectra for all 41 GRBs (thin solid lines) compared to the standard Waxman–Bahcall spectrum for a single burst (thick dotted line). Also shown are the sum of all 41 individual spectra (thick solid line) and the sum of 41 Waxman–Bahcall-like spectra (thick dashed line).

The time window of the prompt emission is determined from the information published in the GCN circulars and reports and checked against the measured γ-ray emission curves (available from NASA (2009)). In case of early or late emission outside the window specified by the satellite experiments the window is extended accordingly. The exact window definitions for the bursts are listed in Table 1. In previous publications on stacked searches for neutrinos from GRBs (Achterberg et al. 2007, 2008) it was assumed that the sum of all GRB spectra follows a Waxman–Bahcall GRB spectrum (Waxman & Bahcall 1997). However, the burst parameters can vary significantly from burst to burst (Guetta et al. 2004; Becker et al. 2006) and the GRB population used here (mostly observed by the *Swift* satellite) is different from the BATSE population on which the calculations from Waxman and Bahcall were based. Therefore, we use the measured parameters to calculate the neutrino spectra for each GRB individually as has already been done in the case of single, bright bursts (Stamatikos et al. 2005; Abbasi et al. 2009b). The parameters (see appendix A) for each GRB are listed in Table 1. In case a parameter has not been measured for a particular burst the average value listed in Table 2 is used. The table also contains assumed values of parameters that have not been measured for any of the GRBs. The resulting neutrino spectra for all 41 GRBs are shown in Figure 1 together with the standard Waxman–Bahcall spectrum[2]. Clear differences in the

[2]The fluence of a standard Waxman–Bahcall burst is calculated from the flux quoted in Waxman (2003) (Equation (17), given as a "diffuse" all-sky flux in $GeV^{-1}\,sr^{-1}\,s^{-1}$) by multiplying it with $4\pi\,sr \times 1\,yr$ and dividing it by the assumed number of bursts per year (667). The resulting fluence is divided by two to account for neutrino oscillations (full mixing assumed).

shapes of the two summed spectra are observed together with an $\mathcal{O}(10)$ times lower overall fluence for the individual spectra. The latter is caused by the much higher sensitivity of *Swift* compared to BATSE. The observed differences stress the importance of using individual fluences in analyses.

2.2. Precursor emission

In the case of precursor emission, the neutrino-producing interactions occur while the fireball is still opaque to electromagnetic emission. Therefore, no analogous photons are observed and modeling of the emission on a per burst basis is not possible. We therefore use the fluence derived by Razzaque et al. (2003) for H-progenitor stars and assume that all 41 GRBs have such a precursor phase with the same fluence. The spectrum is significantly softer than that of the prompt emission. Below 10 TeV, it follows an E^{-2} power law spectrum and has a sharp drop around 60 TeV (see Figure 8). Neutrinos below 60 TeV are mainly produced in interactions of accelerated protons with cold stellar protons whereas those above 60 TeV originate from proton interactions with photons in the jet. The time window is taken as the 100 s immediately preceding the prompt time window. The window is chosen to be large enough to encompass the predicted emission and a potential delay between the phases.

2.3. Wide window emission

While specific predictions have been made for neutrino emission both before, during, and after the observed γ-ray emission of GRBs, there are many unknown quantities that factor into the calculation of fluence. It is therefore important to search for generic emission of high energy neutrinos in a reasonable time window surrounding the observed bursts. For the first time, we perform such a search in a wide time window (-1 h to $+3$ h) around each burst. The size of the window is motivated by possible precursor and afterglow emission, and limited by the requirement to keep backgrounds low. Rather than attempt to model the emission, we assume a generic E^{-2} energy spectrum. Such a spectrum is in agreement with the assumed parent cosmic-ray spectrum and is distinguishable from the atmospheric neutrino background (see Section 5).

3. Detector and data acquisition

IceCube (Achterberg et al. 2006), the successor of the AMANDA experiment and the first next-generation neutrino telescope, is currently being installed in the deep ice at the geographic South Pole. Its final configuration will instrument a volume of about 1 km^3 of clear ice in depths between 1450 m and 2450 m. Neutrinos are reconstructed by detecting the Cherenkov light from charged secondary particles, which are produced in interactions of the neutrinos with the nuclei in the ice or the bedrock below. The optical sensors, known as Digital Optical Modules (DOMs), consist

of a 25 cm Hamamatsu photomultiplier tube (PMT) housed in a pressure-resistant glass sphere and associated electronics (Abbasi et al. 2009a). They are mounted on vertical strings where each string carries 60 DOMs. The final detector will contain 86 such strings spaced horizontally at approximately 125 m intervals[3]. Physics data taking with IceCube started in 2006 with 9 strings installed. The completion of the detector construction is planned for the year 2011. The analyses described here use data taken with the 22-string configuration of the detector, which operated between 2007 May 31 and 2008 April 5.

The data acquisition (DAQ) system of IceCube (Abbasi et al. 2009a) is based on local coincidences of photon signals (hits, threshold 0.25 photo-electrons) in neighboring or next-to-neighboring DOMs on a string within $1\,\mu$s. All data from DOMs belonging to a local coincidence are read out and the digitized waveforms are sent to a computer farm at the surface. In order to pass the trigger a minimum number of 8 DOMs in local coincidences within a time window of $5\,\mu$s is required. If this condition is fulfilled the waveforms are combined to an event and the number and arrival times of the Cherenkov photons are extracted. Here, the relative timing resolution of photons within an event is about 2 ns. The absolute time of an event is determined by a GPS clock to a precision of $\mathcal{O}(\mu\mathrm{s})$, which is more than sufficient for our analyses.

Data are transferred from the South Pole to a computer center in the North via satellite. For the analyses described in this paper we consider only muons produced in charged current interactions

$$\nu_\mu + N \rightarrow \mu + X \tag{1}$$

as only the track-like hit pattern of muons allows for a good angular resolution. In order to fit satellite bandwidth restrictions, a filter removes events which do not qualify as good upgoing neutrino candidates[4]. For this purpose, an initial track is reconstructed for each event using the line-fit algorithm (Ahrens et al. 2004). This is a simple but fast analytic track reconstruction based on the measured hit times in the DOMs. The transferred data forms the basis for our analyses.

4.   Data sets and reconstruction

For our analyses we use data taken with the IceCube detector in its 22-string configuration from 2007 June 1 to 2008 April 4. To prevent bias in our analyses, the data within the -1 h to $+3$ h windows (on-time data) are initially only checked for detector stability until all parameters of the analysis have been fixed, i.e. they are not used in the optimization of the analyses. The remaining off-time data that pass basic quality criteria (95% of all the data collected in the 22-string configuration) amounts to 268.9 days of livetime. This long off-time window allows for a precise

---

[3]Six of these strings will make up a dense subarray in the clearest ice known as Deep Core, extending the sensitivity of IceCube at lower energies.

[4]All triggered data are stored on tape and shipped to the North during the Summer season.

experimental determination of the background rate in the on-time windows.

In addition to the basic quality criteria, the on-time data is tested for stability by fitting a Gaussian to the distribution of low level event counts in each one second bin. In order to check for unexpected periods of dead time, an exponential is fit to the distribution of time delays between events. Data with deviations from the expected shapes are inspected more closely for possible causes which make the data unsuitable for our analysis. Here, most observed deviations can be attributed to transitions between runs and are therefore not critical. Out of 48 northern hemisphere bursts in the time period under investigation, the data for seven do not pass the stability/quality criteria or have gaps during the prompt/precursor emission windows. For all remaining 41 GRBs, both tests show excellent agreement with no indications of abnormal behavior of the detector during the on-time periods. The on-time data cover 100% of the prompt and precursor windows for the 41 selected bursts. For the extended window seven out of the 41 bursts exhibit gaps at the beginning and/or end of the window. For these seven bursts the extended window is shortened accordingly (see Table 3). With this correction, the data cover 94% of the extended time windows of all GRBs. The missing 6% are due to larger gaps in data taking.

After the data has been transferred to the North, a more precise determination of the direction of an event is achieved by fitting a muon-track hypothesis to the hit pattern of the recorded Cherenkov light in the detector using a log-likelihood reconstruction method (Ahrens et al. 2004). A fit of a paraboloid to the region around the minimum in the log-likelihood function yields an estimate of the uncertainty on the reconstructed direction (Neunhöffer 2006). At this point, the data sample with an event rate of $3.3\,\mathrm{Hz}$ is still dominated by several orders of magnitude by misreconstructed downgoing atmospheric muons as demonstrated in Figure 2, which shows a comparison between data and Monte Carlo (see Section 5). The quantities shown are later used to reject these misreconstructed atmospheric muons and improve the sensitivity of the analyses.

- θ_{rec}: reconstructed zenith angle[5];
- σ_{dir}: the uncertainty on the reconstructed track direction (quadratic average of the minor and major axis of the 1σ error ellipse);
- L_{red}: log of the likelihood value of the reconstructed track divided by the number of degrees of freedom (number of hit DOMs minus number of fit parameters). This has proven to be a powerful variable for separating signal and background as visible from Figure 2;
- $L_{U/D}$: difference in log-likelihood value between the reconstructed track and one containing a bias to be reconstructed as downgoing. The bias is zenith angle dependent and follows the rate of downgoing atmospheric muons. The rationale behind this is that a track is much more likely to originate from an atmospheric muon than from a muon generated in a neutrino interaction. Only high-quality upgoing tracks have high $L_{U/D}$ values;
- N_{dir}: the number of photons detected within a -15 to $+75\,\mathrm{ns}$ time window with respect to the

---

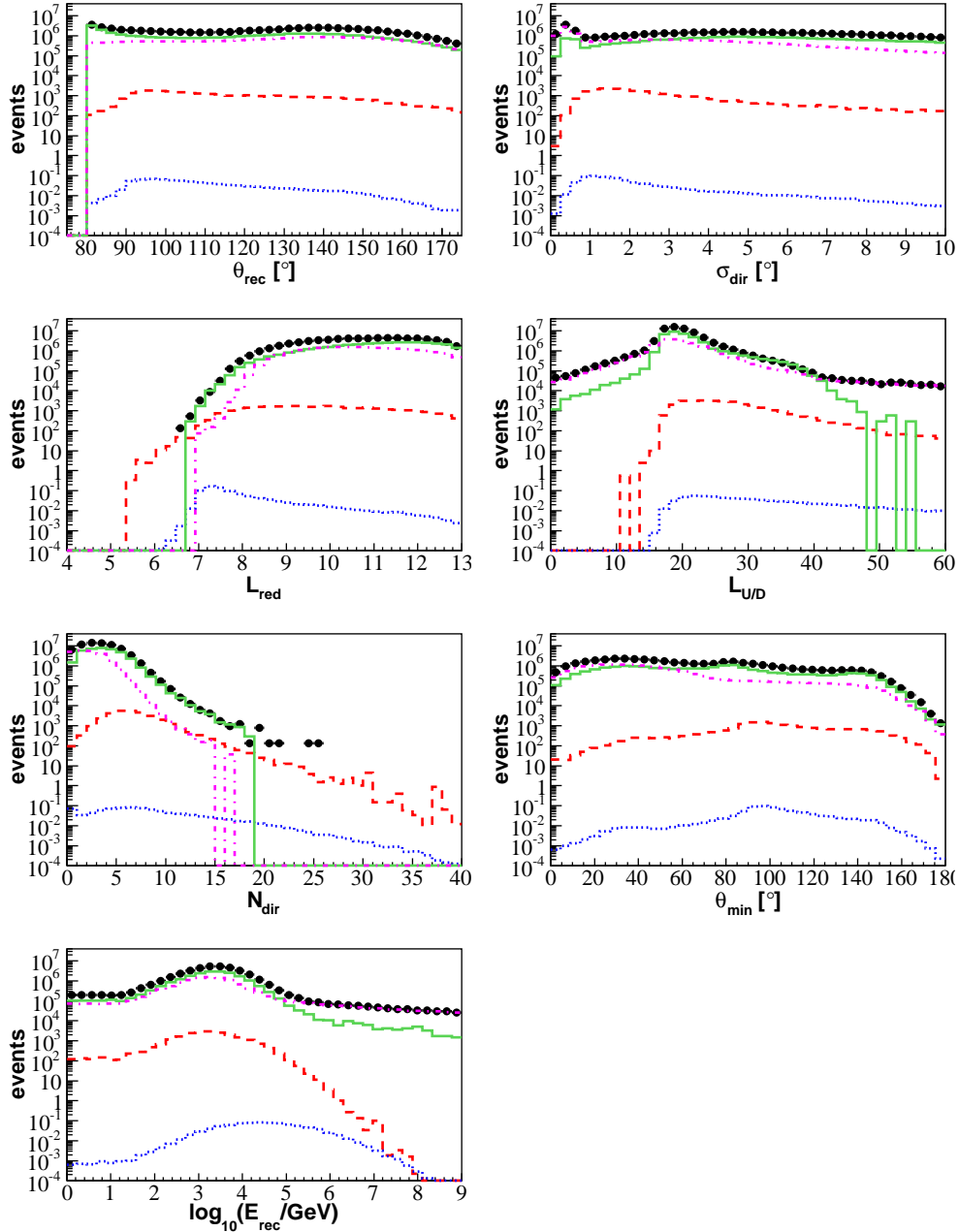[5]The zenith angle in detector coordinates is related to declination δ by $\theta = \delta + 90°$.

Fig. 2.— Comparison between data (black solid circles; 268.9 days of livetime) and simulations in the quality parameters used to reject misreconstructed atmospheric muons at filter level (see Section 3). Monte Carlo shown includes atmospheric muons (green solid lines), coincident muons (magenta dot-dashed lines), atmopheric neutrinos (red dashed lines), and prompt GRB neutrinos (blue dotted lines). The GRB signal is assumed to follow a standard Waxman–Bahcall spectrum and is normalized to the summed expectation from 41 bursts..

expected arrival time for unscattered photons from the muon track hypothesis;

- $\theta_{\min}$: minimum zenith angle from a fit of a two-track hypothesis to the light pattern. For this, the light pattern is divided into two separate sets of hits based on the mean hit time of the event, and a track hypothesis is fitted to each hit set separately. A cut on the smaller zenith angle, $\theta_{\min}$, of the two tracks is very effective against so-called *coincident muons*, where two muons from different atmospheric showers pass the detector in fast succession mimicking an upgoing track. In this case, often at least one of the two tracks is reconstructed as downgoing whereas for good-quality upgoing neutrinos both tracks appear most often as upgoing; and

- $E_{\rm rec}$: reconstructed muon energy at point of closest approach to the center of gravity of hits in an event (Zornoza et al. 2008). This is the calibrated output of a likelihood reconstruction method evaluating the measured number of photons in each DOM with respect to the corresponding probability density function (PDF) of a given track-energy hypothesis.

Muons carry a significant fraction of the original neutrino energy, and at the energies of highest acceptance in our analyses ($\sim 100 \, {\rm TeV}$), have a range of about $10 \, {\rm km}$. The dominant energy loss mechanisms for these muons are Bremsstrahlung and pair production which grow with increasing energy, thereby increasing the amount of Cherenkov light emitted and allowing one to estimate the muon energy.

5. Simulation

Signal neutrinos are generated from the direction of the GRB with the corresponding spectrum using a port of the ANIS code (Gazizov & Kowalski 2005) called NEUTRINO-GENERATOR. Here, the change in position of the source in the detector coordinate system during the respective time window is taken into account. The neutrino emission is assumed to be constant during this time. In addition, three types of background are simulated. At the beginning of the analysis chain, the data sample is dominated by downgoing atmospheric muons, produced by interactions of cosmic rays in the atmosphere, which are reconstructed as upgoing. As more cuts are applied the data sample starts to be dominated by *coincident muon* events. Both event classes are simulated with the CORSIKA air shower simulation package (Heck et al. 1998). Finally, we consider the irreducible background of atmospheric neutrinos generated in the same interactions as the atmospheric muons. These neutrinos are simulated as an all-sky flux with NEUTRINO-GENERATOR and weighted according to the Bartol spectrum (Barr et al. 2004).

Neutrinos are tracked from the surface through the Earth taking into account absorption, scattering and neutral current regeneration of neutrinos (Gazizov & Kowalski 2005). Information on the structure of the Earth is taken from the Preliminary Reference Earth Model (Dziewonski & Anderson 1981). Muons originating from neutrino interactions near the detector and atmospheric muons are traced through rock and ice taking into account continuous and stochastic energy losses (Chirkin & Rhode 2004). The photon signal in the DOMs is determined from a detailed simulation

Table 3.   Modified Extended Time Window for GRBs with Gaps in Data Coverage at Beginning
or End of $-1\,$h to $+3\,$h Window

	$T_1' - T_0$ [s]	$T_2' - T_0$ [s]
GRB070610	-1593	$+10800$
GRB070714B	-3600	$+3930$
GRB071021	-3600	$+5391$
GRB071109	-3022	$+10800$
GRB080205	-3600	$+6289$
GRB080211	-3600	$+8399$
GRB080320	-389	$+8440$

Table 4.   Number of Signal and Background (Off-Time Data) Events for the Unbinned Method
at Different Cut Levels

	Prompt Window		Precursor Window		Wide Window	
Cut Level	No. Events	ϵ^{a} (%)	No. Events	ϵ^{a} (%)	No. Events[b]	ϵ^{a} (%)
			Signal			
Filter	0.062	100	1.8	100	7.6	100
Final	0.033	53	0.53	29	2.8	37
			Background			
Filter[c]	7.6×10^{8}	100	7.6×10^{8}	100	7.6×10^{8}	100
Final[c]	4846	6.5×10^{-4}	4846	6.5×10^{-4}	4846	6.5×10^{-4}
Final (Window)[d]	6.1×10^{-4}	8.2×10^{-11}	6.1×10^{-4}	8.2×10^{-11}	8.8×10^{-2}	1.2×10^{-8}

[a]Efficiency relative to filter level.

[b]For a fluence equal to the computed upper limit in Section 7.

[c]All events after cuts.

[d]Expected events in cones with radii of 2.3° (contain 70% of signal events; see Figure 4) around GRBs within respective time window (prompt: $T_2 - T_1$ from Table 1; precursor: 100 s; wide: 4 h). Note, that these cones are *not* used in the evaluation of the data with the unbinned likelihood method.

of the propagation of Cherenkov light from muons and showers through the ice (Lundberg et al. 2007) which includes the modeling of the changes in absorption and scattering length with depth due to dust layers (Ackermann et al. 2006). This is followed by a simulation of the DOM electronics and the trigger. The simulated DOM signals are then processed in the same way as the data.

6. Data analysis

Muon neutrinos from GRBs show up as an excess of tracks above the background from the direction of the GRB within a certain time window. Background from misreconstructed atmospheric muons can be suppressed by applying quality cuts on reconstructed quantities. Background from atmospheric neutrinos on the other hand is indistinguishable from cosmic neutrinos. Hence, once a high-purity (atmospheric) neutrino sample has been selected, quality cuts which aim at rejecting misreconstructed tracks cannot further improve the signal to background ratio. However, as neutrinos from GRBs are expected to exhibit a harder energy spectrum than that of atmospheric neutrinos, information on the muon energy allows to further increase the sensitivity of the analysis to neutrinos from GRBs.

We have analyzed the data both with an unbinned likelihood and a binned method. In order to enhance the chances for a discovery, we do not analyze the 41 GRBs individually but as a population (stacked analysis)[6]. This allows us to set the most stringent limit on the tested models but might not be optimal in other cases, e.g. if one burst has a much higher neutrino fluence relative to the rest of the GRBs than expected. Also, in case of a discovery a stacked analysis only allows one to calculate the neutrino fluence from the whole burst population but not from individual GRBs. In the following we describe the unbinned likelihood and binned methods and compare their performances in the case of the prompt emission scenario. The more sensitive method is then used to obtain the results presented in Section 7.

6.1. Unbinned log-likelihood method

After filtering at the South Pole and transfer to the North the data sample is still dominated by downgoing muons which are reconstructed as upgoing. These muons are rejected by applying quality cuts on reconstructed quantities (for a description see Section 4).

$$\theta_{\mathrm{rec}} > 85° \ ; \ \sigma_{\mathrm{dir}} < 3° \ ; \ \theta_{\mathrm{min}} > 70° \ ; \ L_{U/D} > 30 \ ; \ L_{\mathrm{red}} \leq \begin{cases} 7.8 & \text{for } N_{\mathrm{dir}} < 7 \\ 8.5 & \text{for } N_{\mathrm{dir}} = 7 \\ 9.5 & \text{for } N_{\mathrm{dir}} > 7 \end{cases} \ . \quad (2)$$

---

[6]In case of the binned method, the numbers of expected and observed events of all GRBs are summed up. In case of the unbinned method, the stacking is performed in Equation (3).

After these cuts, a high-purity upgoing (atmospheric) neutrino sample remains with an event rate of 2.1×10^{-4} Hz. Table 4 lists the cut efficiency for data and signal. A comparison of data with simulations is displayed in Figure 3. In general, good agreement between the atmospheric neutrino Monte Carlo and data is observed. Small deviations for example visible at low N_{dir} are most likely due to atmospheric muon background which is not accounted for by the Monte Carlo due to its limited statistics at this cut level. The cumulative point spread function is shown in Figure 4 (left). The median angular resolution is about $1.5°$. Figure 4 (right) shows the muon neutrino effective area for different declination bands.

The data sets after quality cuts are the starting point for the unbinned likelihood method. In contrast to binned methods where the event is rejected if it lies outside the cut region (binary selection), unbinned likelihood methods do not discard events but use PDFs to evaluate the probability of an event belonging to signal or background population. The unbinned likelihood method used here is similar to that described in Braun et al. (2008). The signal, $S(\vec{x}_i)$, and background, $B(\vec{x}_i)$, PDFs are each the product of a time PDF, a directional PDF, and an energy PDF, where $\vec{x}_i$ denotes the directional, time, and energy variables.

The directional signal PDF is a two-dimensional Gaussian distribution with the two widths being the major and minor axes of the 1σ error ellipse of the paraboloid fit described in Section 4. The time PDF is flat over the respective time window and falls off on both sides with a Gaussian distribution. The width σ of the Gaussian is determined by the length of the time window with a maximum of $\sigma = 25$ s and a minimum of $\sigma = 2$ s. The Gaussian accounts for possible small shifts in the neutrino emission time with respect to that of the γ-rays and prevents discontinuities in the likelihood function. The sensitivity of the method depends only weakly on the exact choice of σ. The energy PDF is determined for each GRB individually. It is derived from the energy-estimator distribution of the tracks of the corresponding signal Monte Carlo data set (weighted to an E^{-2} spectrum[7]) after final cuts (see Equation (2)). The signal PDFs of the GRBs are combined using a weighted sum (Abbasi et al. 2006)

$$S_{\mathrm{tot}}(\vec{x}_i) = \frac{\sum_{j=1}^{N_{\mathrm{GRBs}}} w_j \, S_j(\vec{x}_i)}{\sum_{j=1}^{N_{\mathrm{GRBs}}} w_j} \; , \tag{3}$$

where $S_j(\vec{x}_i)$ is the signal PDF of the jth GRB and w_j is a weight that in the case of the prompt and precursor window is proportional to the expected number of events in the detector according to the fluences described in Section 2. In the case of the extended window we use $w_j = 1$ for all GRBs in order to make the search as general as possible.

---

[7]Using an energy PDF different from that of the assumed signal spectrum cannot lead to an overestimation of the significance of a potential signal as the same PDF is also used to obtain the distribution of background-only samples (see Figure 5) from which the significance is calculated. Studies have shown that for our analyses the loss in discovery potential due to the different PDFs is very small. On the other hand, the softer energy PDF increases the sensitivity to scenarios where the true GRB spectra are softer than assumed.
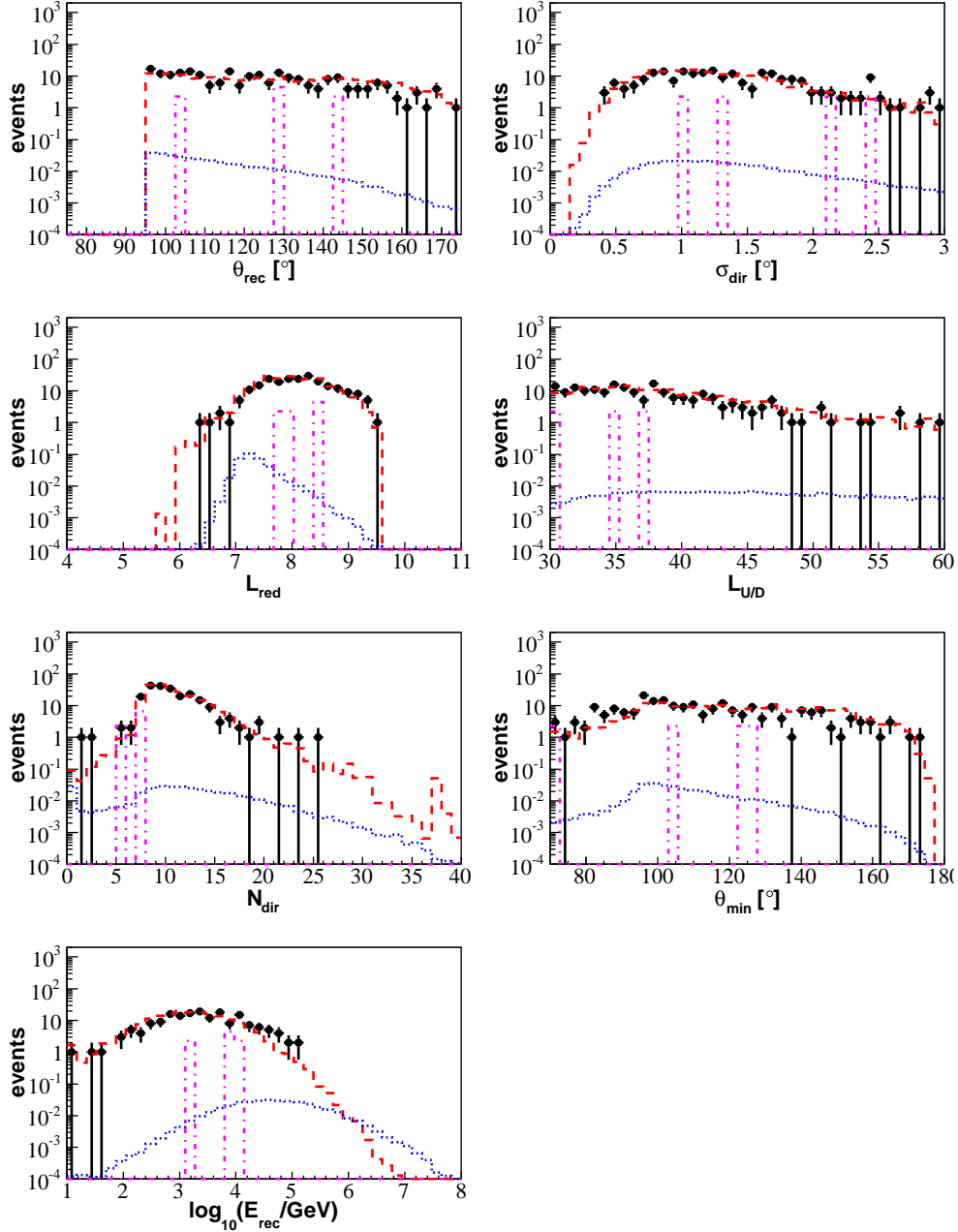
Fig. 3.— Comparison between data (black solid circles; 15.99 days of livetime) and simulations in the quality parameters used to reject misreconstructed atmospheric muons at final cut level. The data includes all data-taking runs with an overlap with the $(-1\,\mathrm{h}$ to $+3\,\mathrm{h})$ extended search windows (this may be considered the maximal on-time of the analysis). Monte Carlo shown includes coincident muons (magenta dot-dashed lines), atmospheric neutrinos (red dashed lines), and prompt GRB neutrinos (blue dotted lines). The simulated single atmospheric muons have been completely removed at this cut level and the statistics for the simulated coincident muons are very low. The GRB signal is assumed to follow a standard Waxman–Bahcall spectrum and is normalized to the summed contribution of 41 bursts.
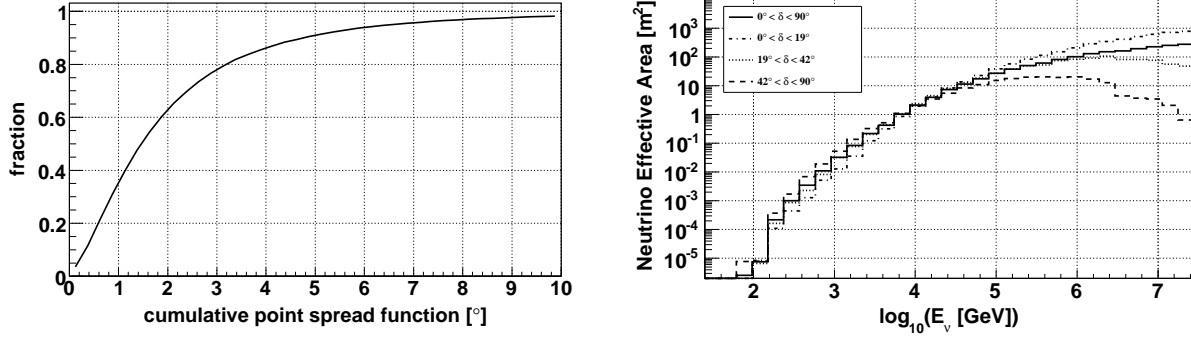
Fig. 4.— Left: Cumulative point spread function for the unbinned method at final cut level. Right: Effective area for muon neutrinos in several declination bands as a function of energy after final event selection in the unbinned method.

For the directional background PDF the detector asymmetries in zenith and azimuth must be taken into account. This is accomplished by evaluating the data in the detector coordinate system. The directional background PDF is hence derived from the distribution of all off-time events after final event selection in the zenith–azimuth plane of the detector. The time distribution of the background during a GRB can be assumed to be constant resulting in a flat time PDF. The energy PDF is determined in the same way as for the signal PDF with weights corresponding to the Bartol atmospheric neutrino flux.

All PDFs are combined in an extended log-likelihood function (Barlow 1989)

$$\ln\left(\mathcal{L}(\langle n_s \rangle)\right) = -\langle n_s \rangle - \langle n_b \rangle + \sum_{i=1}^{N} \ln\left(\langle n_s \rangle\, S_{\text{tot}}(\vec{x}_i) + \langle n_b \rangle\, B(\vec{x}_i)\right) \ , \tag{4}$$

where the sum runs over all reconstructed tracks in the final sample. The variable $\langle n_b \rangle$ is the expected mean number of background events, which is determined from the off-time data set. The mean number of signal events, $\langle n_s \rangle$, is a free parameter which is varied to maximize the expression

$$\ln\left(\mathcal{R}(\langle n_s \rangle)\right) = \ln\left(\frac{\mathcal{L}(\langle n_s \rangle)}{\mathcal{L}(0)}\right) = -\langle n_s \rangle + \sum_{i=1}^{N} \ln\left(\frac{\langle n_s \rangle\, S_{\text{tot}}(\vec{x}_i)}{\langle n_b \rangle\, B(\vec{x}_i)} + 1\right) \tag{5}$$

in order to obtain the best estimate for the mean number of signal events, $\widehat{\langle n_s \rangle}$.

To determine whether a given data set is compatible with the background-only hypothesis 10^8 background data sets for the on-time windows are generated from off-time data by randomizing the track times while taking into account the downtime of the detector. For each of these data sets the $\ln(\mathcal{R})$ value is calculated, yielding the distribution shown in Figure 5. The probability for a data set to be compatible with background is given by the fraction of background data sets with a larger $\ln(\mathcal{R})$ value. For comparison, the plot also displays the $\ln(\mathcal{R})$ distributions for background data sets with one and two injected Monte Carlo signal events, respectively. The signal events
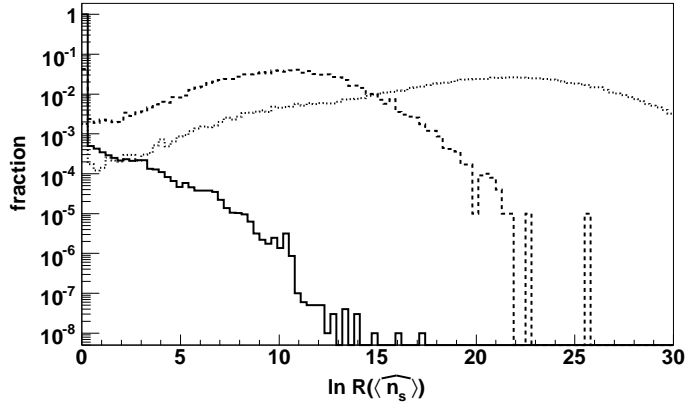
Fig. 5.— Likelihood-ratio distribution of 10^8 randomized background-only data sets for the prompt-window analysis (solid line). Also shown are the corresponding distributions for background data sets with one (dotted) and two (fine dotted) signal events injected. The integrals of all distributions have been normalized to one.

are randomly distributed among the GRBs, where the assignment probability to a specific GRB is proportional to the expected number of events from that burst. The energy of the neutrinos is generated according to the spectra calculated in Section 2.1.

6.2. Binned method

For the binned method, a machine learning algorithm was trained to separate signal and background. The algorithm used was a Support Vector Machine (SVM) (Cortes & Vapnik 1995) with a radial basis function kernel. It was provided with the best reconstructed track direction in detector coordinates as well as many quality parameters including σ_{dir}, L_{red}, $L_{U/D}$, N_{dir}, and θ_{min} which are described in Section 4. The SVM was trained using the off-time filtered data as background and all-sky neutrino simulation weighted to the sum of the individual burst spectra as signal. The optimum SVM parameters (kernel parameter, cost factor, margin) were determined using a coarse, and then fine, grid search with a 5-fold cross validation technique at each node, as described in Hsu et al. (2003).

The resulting SVM classification of events is shown in Figure 6. The final cut on this classifier is optimized to detect a signal fluence with at least 5σ (significance) in 50% of cases (power) by minimizing the Model Discovery Factor (MDF) according to Hill et al. (2006). The MDF is the ratio between the signal fluence required for a detection with the specified significance and power and the predicted fluence. The angular cut around each GRB is then calculated to keep 3/4 of the remaining signal after the cut on the SVM classifier. In this way, there is one cut on the SVM classifier for all GRBs, but different angular cuts around each GRB according to the angular
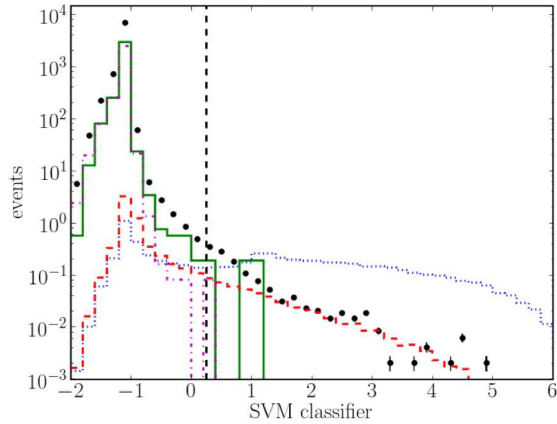
Fig. 6.— The SVM classifier distribution of data (black solid circles) and simulations. Monte Carlo shown includes atmospheric muons (green solid lines), coincident muons (magenta dot-dashed lines), atmospheric neutrinos (red dashed lines), and prompt GRB neutrinos (blue dotted lines). The GRB signal is assumed to follow the summed calculated individual neutrino spectra and is normalized to the rate of atmospheric neutrinos. The vertical dashed line indicates the final optimum cut at 0.25.

resolution of the detector in that direction. The optimum SVM cut is determined to be at a value of 0.25. Table 5 displays the signal and background event rates at different cut levels.

6.3. Comparison of the two methods

We compare the performance of the unbinned likelihood and binned method by means of their discovery potential for the *prompt* neutrino emission scenario. Figure 7 displays for a significance of 5σ the power as a function of the MDF for the two methods. For a power of 50% the unbinned method shows an improvement in the MDF of about a factor 1.8 compared to the binned method. It is therefore used to derive the results presented in the following section. The large gain in sensitivity

Table 5.   Number of Signal and Background (Off-Time Data) Events for the Binned Method in the Prompt Window at Different Cut Levels

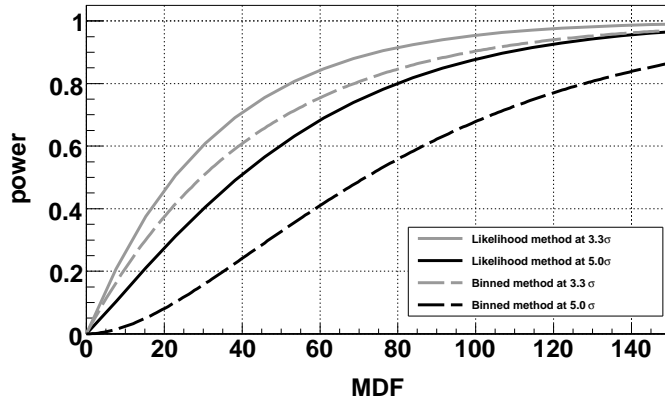| Cut Level | Signal | | Background | |
	No. Events	Efficiency[a] (%)	No. Events	Efficiency[a] (%)
Filter	0.062	100	77×10^7	100
Final	0.023	37	4.7	6.1×10^{-9}

[a]Relative to filter level.

Fig. 7.— Comparison of the discovery potentials of the unbinned likelihood (solid) and binned (dashed) method for significances of 3.3σ (light) and 5σ (dark). Shown is the fraction of data sets yielding at least the stated significance (power) as a function of the ratio between the mean number of injected signal events and the expected number of signal events from the model (MDF).

is partly due to the explicit use of energy information in the likelihood. The discovery potential for the expected fluxes is further improved by weighting the bursts according to the expected number of signal events in the detector in the unbinned method (Equation (3)). In the binned method all bursts are treated equally.

7.   Results and systematic uncertainties

We apply the unbinned likelihood method to the on-time data sets after neutrino candidate event selection with the final cuts (Equation (2)). For all three emission scenarios the values of $\ln(\mathcal{R})$ and $\widehat{\langle n_s \rangle}$ are zero and hence consistent with the null hypothesis. Therefore, we derive 90% CL upper limits[8] on the fluence from the 41 GRBs in the prompt phase of $3.7 \times 10^{-3}\,\mathrm{erg\,cm^{-2}}$ (72 TeV – 6.5 PeV) and on the fluence from the precursor phase of $2.3 \times 10^{-3}\,\mathrm{erg\,cm^{-2}}$ (2.2 TeV – 55 TeV), where the quoted energy ranges contain 90% of the expected signal events in the detector. Further information is listed in Table 6. The limits, which are displayed in Figure 8, are not strong enough to constrain the models. The 90% CL upper limit for the wide time window is $2.7 \times 10^{-3}\,\mathrm{erg\,cm^{-2}}$ (3 TeV – 2.8 PeV) assuming an E^{-2} flux.

To illustrate, we counted the number of events after final cuts in cones with radii 2.3° around the GRB positions (contain 70% of signal events; see Figure 4) within the corresponding time

---

[8]The limits are calculated following a procedure due to Neyman (Neyman 1937; Amsler et al. 2008). The 90% CL upper limit corresponds to the signal flux for which 90% of background data sets with signal events injected according to the calculated GRB spectra yield $\ln(\mathcal{R})$ values greater than the observed one.
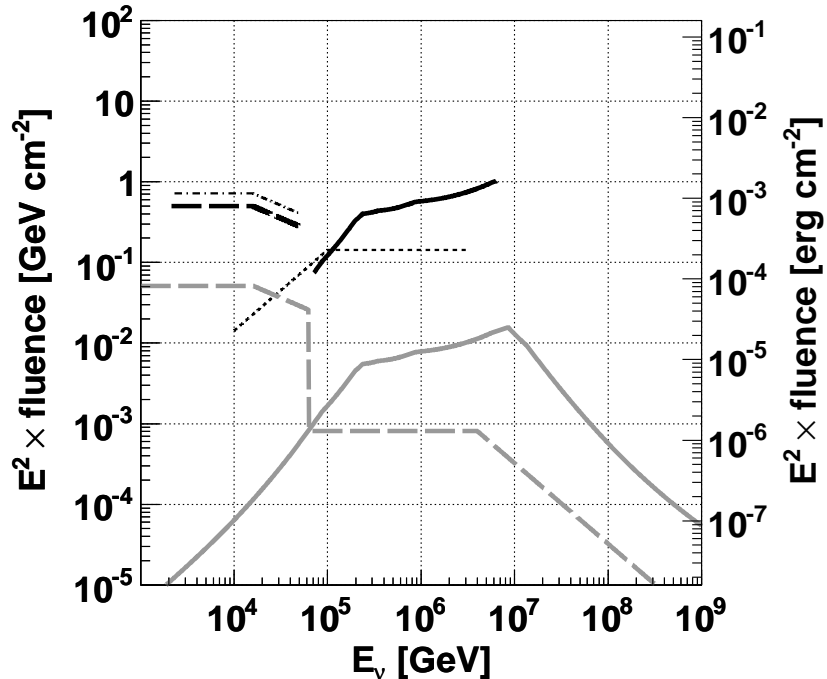
Fig. 8.— 90% CL upper limits (dark thick lines) on the neutrino fluence from the 41 northern hemisphere GRBs for different emission models (light thick lines): precursor (dashed, Razzaque et al. (2003)) and prompt (solid, see Section 2). The dark dotted and dash-dotted thin lines mark the scaled AMANDA 90% CL upper limits (Achterberg et al. 2008; Kuehn 2007) on the prompt and precursor fluences, respectively.

windows (prompt: $T_2 - T_1$ from Table 1 ; precursor: $100\,\mathrm{s}$; wide: $4\,\mathrm{h}$). In addition, we analyzed the data in the prompt window with the binned method after final cuts. In all cases, zero events remain which is consistent with the results of the unbinned likelihood method.

As described previously, we use the off-time data to determine the background rate in the on-time windows. This technique removes many potential sources of uncertainties in the calculation of the significance of a possible signal that are introduced when using a simulation of the background. However, this method makes the assumption that the rate of data during the off-time and on-time windows are the same. Furthermore, we use Monte Carlo for the signal simulation and the derivation of upper limits, which involves the propagation of particles through the Earth and ice, and the simulation of the detector response. The most important sources for systematic uncertainties are discussed below in detail. Their effects on the upper limits are summarized in Table 7.

Ice simulation: Inaccuracies in the ice simulation can lead to a wrong estimate of the efficiency of the detector to neutrinos from GRBs. Data-Monte Carlo comparisons and variation of simulation parameters indicate that the systematic uncertainty from this aspect of the simulation is about $\pm 15\%$.

Table 6.   Summary of Search Results for Prompt and Precursor Window

Window	n_{exp}	n_{limit}	Factor
Prompt Window	0.033	2.4	72
Precursor Window	0.26	2.5	9.7
Wide Time Window	–	2.7	–

Note. — n_{exp}: number of expected events in the detector after final cuts from all 41 GRBs in the unbinned search; n_{limit}: 90% CL upper limit on the event number from all 41 GRBs; factor: factor by which the limit exceeds the predicted event number n_{exp}.

Table 7.   Summary of Effects of Systematic Uncertainties on the Upper Limits

Type of Uncertainty	Prompt Window	Precursor Window	Extended Window
Ice Simulation	±15%	±15%	±15%
DOM Efficiency	±5%	±10%	±7%
Lepton Propagation	±5%	±5%	±5%
Background Rate	< 1%	< 1%	< 1%
Sum	±17%	±19%	±17%

DOM efficiency: A ±10% uncertainty in the efficiency of the optical modules in the detection of photons leads to a corresponding uncertainty in the number of expected events from a GRB. This effect is nonlinear and spectrally dependent, so simulation was generated spanning the range of uncertainties to determine the resulting change in signal event rates;

Neutrino and muon propagation: Theoretical uncertainties on muon energy losses and the neutrino-nucleon cross-section, determined from the uncertainty on the CTEQ6 PDFs (Pumplin et al. 2002), contribute a 5% uncertainty on the neutrino event rate in the detector;

Background rate: After final cuts the variation of the event rate over the data taking period is about ±5%. In order to account for potential differences at the time of the bursts the background data rate is varied by this amount. This results in a shift of the upper limits of less than ±1% and is therefore negligible.

8. Comparison to other results

A search with the AMANDA detector for muon neutrinos in the prompt and precursor phase was conducted for GRBs detected between 1997 and 2003 (Achterberg et al. 2008) with null result. The analysis of prompt neutrinos contained 419 bursts observed by the BATSE experiment (Paciesas et al. 1999) as well as by others with similar characteristics. The large number of bursts allowed that analysis to set an upper limit only a factor 1.4 above the prediction of the Waxman–Bahcall prompt emission model. A further search with the AMANDA detector for muon neutrinos was conducted for 85 GRBs detected between 2005 and 2006 (Strahler 2009), primarily by the *Swift* satellite, also with null result. Due to the smaller number of bursts, the upper limit from this analysis is much less restrictive. Converting the upper limit obtained from the 419 bursts to a fluence limit from 41 standard Waxman–Bahcall bursts (for definition see footnote 2) yields the dotted line in Figure 8. Due to the 10 times smaller number of bursts available, the limit presented in this paper is about a factor three worse. For the precursor emission model, the AMANDA limit (Achterberg et al. 2008; Kuehn 2007) is much less restrictive as only 60 bursts, detected between 2001 and 2003, were used. It is shown in Figure 8 as a dash-dotted line. Here, our analysis improves on the AMANDA upper limit despite the fact that 30% fewer bursts were investigated.

The AMANDA data were also analyzed for neutrinos of all flavors from GRBs (Achterberg et al. 2007). Apart from a search for neutrinos from 73 bursts detected by BATSE in 2000, another search did not rely on information from satellites but looked for a clustering of events within sliding time windows of 1 s and 100 s. Due to this more generic approach and the low number of bursts, respectively, the limits from these analyses are much less restrictive than those from Achterberg et al. (2008). However, the sliding-window or similar searches are the only way to detect GRBs where either the jet does not emerge from the progenitor star (choked bursts, Meszaros & Waxman (2001)) or the γ-ray signal is not observed by satellites for other reasons.

We continue with a discussion of the impact of results from high-energy γ-ray observations on

expected neutrino fluences. Along with high-energy neutrinos which originate from the decay of charged pions, high-energy γ-ray photons are produced in the decay of simultaneously generated neutral pions. In addition, high-energy photons are produced in inverse-Compton scattering of synchrotron photons by accelerated electrons (Falcone et al. 2008). In contrast to neutrinos, the flux of high-energy γ-ray photons at the Earth is significantly reduced due to the large optical depths for photon-photon pair production inside the source for not too large jet Lorentz factors $\Gamma_{\rm jet} \lesssim 800$ (Falcone et al. 2008). In addition, high-energy photons above $100\,{\rm GeV}$ are absorbed on the extragalactic background light (EBL) if they travel distances with $z \gtrsim 0.5$. Observations with air-Cherenkov telescopes like H.E.S.S. (Aharonian et al. 2009; Tam et al. 2009) or MAGIC (Albert et al. 2007; Galante et al. 2009) are also hampered by the fact that usually it takes more than $50\,{\rm s}$ (MAGIC) or $100\,{\rm s}$ (H.E.S.S.) from the observation of a GRB by a satellite to the start of data taking with these telescopes. Therefore, the prompt emission window is only partially covered or not at all. MILAGRO as an air shower array observed large parts of the sky continuously (Atkins et al. 2004, 2005; Abdo et al. 2007). However, it was mostly sensitive to energies above $100\,{\rm GeV}$ and therefore suffered significantly from γ-ray absorption on the EBL. HAWC, the successor of Milagro currently in the planning phase, will be able to detect γ rays from GRBs down to $100\,{\rm GeV}$ where about 50 (*Fermi*) GRBs per year will fall in its field of view (Goodman et al. 2009).

At energies above $100\,{\rm GeV}$, there has been no definitive detection of γ-ray emission from GRBs. Milagrito (Atkins et al. 2000, 2003) and the HEGRA AIROBICC array (Padilla et al. 1998) reported evidence at the 3σ level for high-energy γ-ray emission from GRB 970417A ($E_\gamma > 650\,{\rm GeV}$) and GRB 920925C ($E_\gamma > 20\,{\rm TeV}$), respectively. However, subsequent searches for high-energy γ-ray emission from GRBs did not find similar signals. The limits obtained from MAGIC and H.E.S.S. are not directly comparable to our results due to their incomplete burst coverage. In Atkins et al. (2004), Atkins et al. (2005) and Abdo et al. (2007) the MILAGRO collaboration reports 99% CL upper limits for a large number of individual bursts (both long and short) between 2000 and 2006 down to $10^{-7}\,{\rm erg\,cm^{-2}}$ (energy range $\sim 100\,{\rm GeV} - 10\,{\rm TeV}$; the exact energy range differs from publication to publication). Extrapolating the average per burst 99% CL upper limit for the prompt window in our analysis to the energy range from $100\,{\rm GeV}$ to $10\,{\rm TeV}$ yields $3.2 \times 10^{-7}\,{\rm erg\,cm^{-2}}$. However, the photon limits do not constrain our results as they do not account for absorption in the EBL (this would significantly worsen the limits) and include an unknown, probably dominant, contribution from inverse-Compton scattering. In general, current flux predictions for high-energy gamma rays from GRBs are near or below the sensitivity of current instruments (Falcone et al. 2008), where the predicted fluxes in the energy range below $\sim 100\,{\rm TeV}$ are dominated by the leptonic emission component in most scenarios.

Within the internal shock (fireball) model, synchrotron self-Compton (SSC) processes between the accelerated electrons and the γ-ray photons could lead to a high-energy γ-ray peak in the GeV range detectable by *Fermi* in case of bright GRBs. Up to now, this has happend only for a handful of bursts (one of the photons with the highest energy from a GRB detected by *Fermi* came from GRB 080916C and had an energy of $\sim 13\,{\rm GeV}$ (Abdo et al. 2009)). However, this does

not necessarily disfavor the internal shock scenario. As discussed in Fan (2009), the amount of energy in high-energy photons could be suppressed by an inefficient SSC process in the extreme Klein-Nishina regime or a combination of a SSC peak at high energies and a low photon cut-off energy above which the fireball becomes optical thick.

9. Conclusions and outlook

We have performed a set of complementary searches for muon neutrinos associated in space and time with 41 gamma-ray bursts that were observed in the northern sky between 2007 June and 2008 April. For the first time in searches with large GRB populations, we have calculated individual prompt neutrino spectra for all 41 GRBs using measured GRB parameters. The search results are consistent with the case of a background-only hypothesis. Therefore, we place 90% CL upper limits on the fluence from the prompt phase of $3.7 \times 10^{-3} \, \mathrm{erg \, cm^{-2}}$ ($72 \, \mathrm{TeV} - 6.5 \, \mathrm{PeV}$) and on the fluence from the precursor phase of $2.3 \times 10^{-3} \, \mathrm{erg \, cm^{-2}}$ ($2.2 \, \mathrm{TeV} - 55 \, \mathrm{TeV}$), where the quoted energy ranges contain 90% of the expected signal events in the detector. Though the number of bursts is smaller than in previous searches the larger detector allows us to improve on the limits for the precursor phase by a factor 1.4. Compared to the predictions, the limits lie a factor 72 (prompt phase) and 9.7 (precursor phase) higher. Hence, they do not allow us to constrain the models. Apart from these model-driven searches, we have also conducted for the first time a generic search for neutrino emission from GRBs in a wide window of ($-1 \, \mathrm{h}$ to $+3 \, \mathrm{h}$) around each burst. Finding no evidence for a signal, we place a 90% CL upper limit on the fluence of $2.7 \times 10^{-3} \, \mathrm{erg \, cm^{-2}}$ ($3 \, \mathrm{TeV} - 2.8 \, \mathrm{PeV}$) assuming an E^{-2} flux.

Launched in 2008 June, the *Fermi* Gamma-ray Space Telescope (NASA 2008) has begun to provide an expanded catalog of sources for future neutrino searches. With a much larger field of view than other satellites, *Fermi* has increased the GRB detection rate by more than a factor two. At the same time, the detected bursts have on average a higher luminosity than those detected by *Swift* due to the lower sensitivity of the *Fermi*-GBM (Gamma-ray Burst Monitor) instrument. The first IceCube analysis to take advantage of the increased detection opportunities will utilize the 40-string configuration of the detector, already as large as the full IceCube along one axis. This gives it the full angular resolution power along that direction and thus provides powerful background rejection. However, this is mitigated by the comparatively poor angular resolution of the *Fermi*-GBM ($\sim 3°$), which is worse than the IceCube resolution. With the full 80-string detector scheduled to be completed in 2011 and an expected 100 to 150 detected bursts per year in the northern hemisphere by the *Fermi* and *Swift* satellites the sensitivity of IceCube to neutrinos from GRBs will soon exceed that of AMANDA. This will allow IceCube to either confirm the predicted fluxes within the next years or set stringent limits thereby disfavoring GRBs as the major sources of ultra-high energy cosmic rays.

A. Equations used in the calculation of the neutrino spectra

$$F_\gamma(E_\gamma) = \frac{\mathrm{d}N(E_\gamma)}{\mathrm{d}E_\gamma} = f_\gamma \times \begin{cases} \left(\frac{\epsilon_\gamma}{\mathrm{MeV}}\right)^{\alpha_\gamma} \left(\frac{E_\gamma}{\mathrm{MeV}}\right)^{-\alpha_\gamma} & \text{for } E_\gamma < \epsilon_\gamma \\ \left(\frac{\epsilon_\gamma}{\mathrm{MeV}}\right)^{\beta_\gamma} \left(\frac{E_\gamma}{\mathrm{MeV}}\right)^{-\beta_\gamma} & \text{for } E_\gamma \geq \epsilon_\gamma \end{cases} \tag{A1}$$

$$\mathcal{F}_\gamma = \int \mathrm{d}E_\gamma \ E_\gamma F_\gamma(E_\gamma) \tag{A2}$$

$$F_\nu(E_\nu) = \frac{\mathrm{d}N(E_\nu)}{\mathrm{d}E_\nu} = f_\nu \times \begin{cases} \left(\frac{\epsilon_{\nu,1}}{\mathrm{GeV}}\right)^{\alpha_\nu} \left(\frac{E_\nu}{\mathrm{GeV}}\right)^{-\alpha_\nu} & \text{for } E_\nu < \epsilon_{\nu,1} \\ \left(\frac{\epsilon_{\nu,1}}{\mathrm{GeV}}\right)^{\beta_\nu} \left(\frac{E_\nu}{\mathrm{GeV}}\right)^{-\beta_\nu} & \text{for } \epsilon_{\nu,1} \leq E_\nu < \epsilon_{\nu,2} \\ \left(\frac{\epsilon_{\nu,1}}{\mathrm{GeV}}\right)^{\beta_\nu} \left(\frac{\epsilon_{\nu,2}}{\mathrm{GeV}}\right)^{\gamma_\nu-\beta_\nu} \left(\frac{E_\nu}{\mathrm{GeV}}\right)^{-\gamma_\nu} & \text{for } E_\nu \geq \epsilon_{\nu,2} \end{cases} \tag{A3}$$

$$\epsilon_1 = 7 \times 10^5 \,\mathrm{GeV} \ \frac{1}{(1+z)^2} \left(\frac{\Gamma_{\mathrm{jet}}}{10^{2.5}}\right)^2 \left(\frac{\mathrm{MeV}}{\epsilon_\gamma}\right) \tag{A4}$$

$$\epsilon_2 = 10^7 \,\mathrm{GeV} \ \frac{1}{1+z} \ \sqrt{\frac{\epsilon_e}{\epsilon_B}} \ \left(\frac{\Gamma_{\mathrm{jet}}}{10^{2.5}}\right)^4 \left(\frac{t_{\mathrm{var}}}{0.01\,\mathrm{s}}\right) \ \sqrt{\frac{10^{52}\,\mathrm{erg\,s^{-1}}}{L_\gamma^{\mathrm{iso}}}} \tag{A5}$$

$$\alpha_\nu = 3 - \beta_\gamma \quad, \quad \beta_\nu = 3 - \alpha_\gamma \quad, \quad \gamma_\nu = \beta_\nu + 2 \tag{A6}$$

$$\frac{\Delta R}{\lambda_{p\gamma}} = \left(\frac{L_\gamma^{\mathrm{iso}}}{10^{52}\,\mathrm{erg\,s^{-1}}}\right) \left(\frac{0.01\,\mathrm{s}}{t_{\mathrm{var}}}\right) \left(\frac{10^{2.5}}{\Gamma_{\mathrm{jet}}}\right)^4 \left(\frac{\mathrm{MeV}}{\epsilon_\gamma}\right) \tag{A7}$$

$$\int_0^\infty \mathrm{d}E_\nu \ E_\nu F_\nu(E_\nu) = \frac{1}{8} \ \frac{1}{f_e} \ \left(1 - (1 - \langle x_{p\to\pi}\rangle)^{\Delta R/\lambda_{p\gamma}}\right) \int_{1\,\mathrm{keV}}^{10\,\mathrm{MeV}} \mathrm{d}E_\gamma \ E_\gamma F_\gamma(E_\gamma) \tag{A8}$$

- Parameters of the γ-ray spectrum $F_\gamma(E_\gamma)$:
  - ϵ_γ: break energy;
  - α_γ: spectrum index before break energy;
  - β_γ: spectrum index after break energy;
  - $\mathcal{F}_\gamma$: measured fluence in γ-rays integrated over the energy range given in the GCN circulars and reports (NASA 2009);
  - f_γ: normalization; obtained from integral of Equation (A2).

- Parameters of the neutrino spectrum $F_\nu(E_\nu)$:
  - ϵ_1: first break energy;
  - ϵ_2: second break energy;
  - α_ν: spectrum index before first break energy;
  - β_ν: spectrum index between frist and second break energy;
  - γ_ν: spectrum index after second break energy;
  - f_ν: normalization; obtained from integral of Equation (A8).

- z: redshift of GRB;
- ϵ_e: fraction of jet energy in electrons;
- ϵ_B: fraction of jet energy in magnetic field;
- f_e: ratio between energy in electrons and protons;
- L_γ^{iso}: isotropic luminosity of the GRB;
- t_{var}: variability of the γ-ray light curve of the GRB;
- Γ_{jet}: Lorentz boost factor of the jet.

   The expression $1 - (1 - \langle x_{p\to\pi}\rangle)^{\Delta R/\lambda_{p\gamma}}$ in Equation (A8) estimates the overall fraction of the proton energy going into pions from the size of the shock, ΔR, and the mean free path of a proton for photomeson interactions, $\lambda_{p\gamma}$. Here, $\langle x_{p\to\pi}\rangle = 0.2$ is the average fraction of proton energy transferred to a pion in a single interaction. The expression ensures that the transferred energy fraction is ≤ 1. The calculations are insensitive to the beaming effect caused by a narrow opening angle of the jet as all formulae contain the isotropic luminosity in conjunction with a 4π shell geometry, i.e. effectively use luminosity per steradian. For example, the target photon density used to calculate N_{int} is given by $n_\gamma \propto L_\gamma^{\mathrm{iso}}/4\pi R^2$, where R is the distance of the shock region from the central black hole.

REFERENCES

Abbasi, R., (HiRes Collaboration), et al. 2006, ApJ, 636, 680, arXiv:astro-ph/0507120

Abbasi, R., (IceCube Collaboration), et al. 2009a, Nucl. Inst. Meth. A, 601, 294, arXiv:0810.4930

—. 2009b, ApJ, 701, 1721, arXiv:0902.0131

Abdo, A. A., (Fermi LAT and Fermi GBM Collaboration), et al. 2009, Science, 323, 1688

Abdo, A. A., (Milagro Collaboration), et al. 2007, ApJ, 666, 361

Achterberg, A., (IceCube Collaboration), et al. 2006, Astropart. Phys., 26, 155, arXiv:astro-ph/0604450

—. 2007, ApJ, 664, 397, arXiv:astro-ph/0702265

—. 2008, ApJ, 674, 357, arXiv:0705.1186

Ackermann, M., (AMANDA Collaboration), et al. 2006, J. Geophys. Res., 111, D13203

Aharonian, F., (H.E.S.S. Collaboration), et al. 2009, ApJ, 690, 1068, arXiv:0809.2334

Ahrens, J., (AMANDA Collaboration), et al. 2004, Nucl. Inst. Meth. A, 524, 169, astro-ph/0407044

Albert, J., (MAGIC Collaboration), et al. 2007, ApJ, 667, 358

Alvarez-Muniz, J., & Halzen, F. 1999, ApJ, 521, 928, arXiv:astro-ph/9902039

Amsler, C., et al. 2008, Phys. Lett. B, 667, 1

Athar, H., Kim, C. S., & Lee, J. 2006, Mod. Phys. Lett. A, 21, 1049, arXiv:hep-ph/0505017

Atkins, R. W., (Milagro Collaboration), et al. 2000, ApJ, 533, L119

—. 2003, ApJ, 583, 824

—. 2004, ApJ, 604, L25

—. 2005, ApJ, 630, 996

Barlow, R. J. 1989, Statistics (Chichester, West Sussex: Wiley)

Barr, G. D., et al. 2004, Phys. Rev. D, 70, 023006, arXiv:astro-ph/0403630

Becker, J. K. 2008, Phys. Rep., 458, 173

Becker, J. K., Stamatikos, M., Halzen, F., & Rhode, W. 2006, Astropart. Phys., 25, 118, arXiv:astro-ph/0511785

Braun, J., Dumm, J., de Palma, F., Finley, C., Karle, A., & Montaruli, T. 2008, Astropart. Phys., 29, 299, arXiv:0801.1604

Burrows, D. N., et al. 2005, Space Sci. Rev., 120, 165, arXiv:astro-ph/0508071

—. 2007, Phil. Trans. Roy. Soc. A, 365, 1213, arXiv:0810.4930

Chirkin, D., & Rhode, W. 2004, arXiv:hep-ph/0407075

Cortes, C., & Vapnik, V. 1995, Machine Learning, 20, 273

Dziewonski, A. M., & Anderson, D. L. 1981, Phys. Earth. Planet. Int., 25, 297

Eichler, D., Livio, M., Piran, T., & Schramm, D. N. 1989, Nature, 340, 126

Falcone, A. D., et al. 2008, arXiv:0810.0520

Fan, Y. Z. 2009, Mon. Not. R. Astron. Soc., accepted, arXiv:0905.0908

Galante, N., (MAGIC Collaboration), et al. 2009, in AIP Conf. Proc., ed. F. A. Aharonian, W. Hofmann, & F. Rieger, Vol. 1085 (Melville, NY: AIP), 411

Gazizov, A., & Kowalski, M. O. 2005, Comp. Phys. Comm., 172, 203, arXiv:astro-ph/0406439

Goodman, J., (Milagro Collaboration), (HAWC Collaboration), et al. 2009, in , Łódź, Poland, to be published in Proc. of the 31th Int. Cosmic Ray Conf.

Guetta, D., Hooper, D., Alvarez-Muniz, J., Halzen, F., & Reuveni, E. 2004, Astropart. Phys., 20, 429

Heck, D., et al. 1998, CORSIKA: A Monte Carlo Code to Simulate Extensive Air Showers, Tech. Rep. FZKA 6019, Forschungszentrum Karlsruhe

Hill, G. C., Hodges, J., Hughey, B., Karle, A., & Stamatikos, M. 2006, in Statistical Problems in Particle Physics, Astrophysics and Cosmology: PHYSTAT 2005, ed. L. Lyons & M. Karagoz (Unel. London, England: Imperial Coll. Press), 108

Hsu, C.-W., Chang, C.-C., & Lin, C.-J. 2003, A Practical Guide to Support Vector Classification, Tech. rep., Department of Computer Science, National Taiwan University

IPN. 1990, IPN3 homepage, http://www.ssl.berkeley.edu/ipn3/

Kuehn, K. 2007, PhD thesis, University of California-Irvine

Learned, J. G., & Pakvasa, S. 1995, Astropart. Phys., 3, 267

Lundberg, J., et al. 2007, Nucl. Inst. Meth., A581, 619, arXiv:astro-ph/0702108

Mereghetti, S. 2004, in Gamma-ray Bursts: 30 Years of Discovery: Gamma-Ray Burst Symposium, ed. E. E. Fenimore & M. Galassi, Vol. 727 (Melville, NY: AIP), 607, arXiv:astro-ph/0312340

Meszaros, P., & Rees, M. J. 1993, ApJ, 405, 278

Meszaros, P., & Waxman, E. 2001, Phys. Rev. Lett., 87, 171102

Murase, K., & Nagataki, S. 2006, Phys. Rev. Lett., 97, 051101, arXiv:astro-ph/0604437

Narayan, R., Paczynski, B., & Piran, T. 1992, ApJ, 395, L83, arXiv:astro-ph/9204001

NASA. 1994, Konus-Wind homepage, http://heasarc.gsfc.nasa.gov/docs/heasarc/missions/wind.html

—. 2008, Fermi homepage, http://www.nasa.gov/mission_pages/GLAST/main/index.html

—. 2009, GCN: The Gamma ray bursts Coordinates Network, http://gcn.gsfc.nasa.gov

Neunhöffer, T. 2006, Astropart. Phys., 25, 220

Neyman, J. 1937, Phil. Trans. Roy. Soc., 236, 333

Paciesas, W. S., et al. 1999, Astrophys. J. Suppl., 122, 465, arXiv:astro-ph/9903205

Padilla, L., et al. 1998, A&A, 337, 43, arXiv:astro-ph/9807342

Pumplin, J., Stump, D. R., Huston, J., Lai, H. L., Nadolsky, P. M., & Tung, W. K. 2002, J. High Energy Phys., 0207, 012

Razzaque, S., Meszaros, P., & Waxman, E. 2003, Phys. Rev. D, 68, 083001

Rees, M. J., & Meszaros, P. 1994, ApJ, 430, L93

Sari, R., & Piran, T. 1997, ApJ, 485, 270, arXiv:astro-ph/9701002

Stamatikos, M., (IceCube Collaboration), et al. 2005, in Proc. Int. Cosmic Ray Conf. (ICRC'05), ed. B. S. Acharya, S. Gupta, P. Jagadeesan, A. Jain, S. Karthikeyan, S. Morris, & S. Tonwar, Vol. 4 (Colaba, Mumbai: Tata Institute of Fundamental Research), 471, arXiv:astro-ph/0510336

Strahler, E. 2009, PhD thesis, University of Wisconsin-Madison

Tam, P., Chadwick, P., Gallant, Y., Horns, D., Puhlhofer, G., Rowell, G., Wagne, S., (H.E.S.S. Collaboration), et al. 2009, arXiv:0902.1561

Tavani, M., et al. 2008, Nucl. Inst. Meth. A, 588, 52

Vietri, M. 1995, ApJ, 453, 883, arXiv:astro-ph/9506081

Waxman, E. 1995, Phys. Rev. Lett., 75, 386

—. 2003, Nucl. Phys. B-Proc. Suppl., 118, 353, arXiv:astro-ph/0211358

Waxman, E., & Bahcall, J. N. 1997, Phys. Rev. Lett., 78, 2292, arXiv:astro-ph/9701231

—. 2000, ApJ, 541, 707

Woosley, S. E. 1993, ApJ, 405, 273

Zornoza, J., Chirkin, D., (IceCube Collaboration), et al. 2008, in Proc. of the 30th Int. Cosmic Ray Conf., ed. L. Nellen, F. A. Sánchez, & J. F. Valdés-Galicia, Vol. 5 (Mexico City, Mexico: Universidad Nacional Autónoma de México), 1275, arXiv:0711.0353